Icarus 390 (2023) 115326

Contents lists available at ScienceDirect

Icarus

journal homepage: www.elsevier.com/locate/icarus

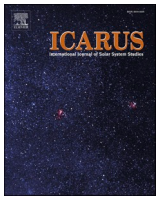

Investigation of the shocked Viñales ordinary chondrite (L6) meteorite fall – Implications for shock classification, fragmentation, and collision dynamics

I.P. Baziotis [a,*], S. Xydous [a], A. Papoutsa [a], J. Hu [b], C. Ma [b], L. Ferrière [c], S. Klemme [d], J. Berndt [d], P.D. Asimow [b]

[a] Agricultural University of Athens, Iera Odos 75, 11855 Athens, Greece
[b] California Institute of Technology, Division of Geological and Planetary Sciences, Pasadena, CA 91125, USA
[c] Natural History Museum Vienna, Burgring 7, A-1010 Vienna, Austria
[d] Westfälische Wilhelms-Univ. Münster, Correnstrasse 24, 48149 Münster, Germany

ARTICLE INFO

Keywords:
Viñales meteorite
Ordinary chondrite
Asteroid dynamics
Collision
L-chondrite disruption body

ABSTRACT

The effects of collisions on the evolution of asteroids, ranging from local fracturing to brecciation or even to catastrophic disruption, depend primarily on the encounter velocities. Here we present a refined view of the mineralogy and texture of the recent fall Viñales, an L6 ordinary chondrite meteorite. It preserves features that require at least one energetic impact, including numerous shock melt veins of variable thickness. We report the identification of two high-pressure phases, majorite and albitic jadeite, limited to just one of these shock melt veins. Viñales is a moderately shocked sample, shock stage S4, that experienced a complex and spatially variable pressure-temperature-time history with a low (but non-zero) probability of preservation of high-pressure phases.

1. Introduction

Some ordinary chondrites contain high-pressure (HP) minerals and other impact-related features, such as shock melt veins (MVs) and melt pockets, that yield constraints on shock conditions and hence parameters such as the sizes of colliding bodies and their encounter velocity. The L-chondrites, in particular, commonly record a major shock event ca. 470 Ma ago that is thought to be associated with disruption of the parent body (Bogard et al., 1976; Heymann, 1967; Schmitz et al., 2001; Korochantseva et al., 2007; Yin et al., 2014). The presence of HP minerals formed in shock melt veins may suggest specific pressure and temperature conditions of formation at some time after the achievement of conditions sufficient to induce melting. Known HP phases in ordinary chondrites include dense forms of silicates (ringwoodite and wadsleyite with olivine composition; akimotoite, majorite, and bridgmanite with pyroxene composition; lingunite and albitic jadeite with feldspar composition), oxides (monoxides such as stishovite, mixed oxides such as xieite), metals, sulphides, phosphates (e.g., tuite) and carbon (e.g., impact diamonds) (Binns et al., 1969; Chao et al., 1962; Chen et al., 2003; James, 1969; Liu, 1978; Mason et al., 1968; Ma et al., 2022; Putnis and Price, 1979; Sazonova et al., 2006; Sharp et al., 1997; Tschauner et al., 2014; Xie et al., 2002).

Here, we report our observations on samples of the Viñales L6 ordinary chondrite, an observed fall from February 1st 2019. Hundreds of stones of variable size and weight, >100 kg in total, were recovered shortly after the fall in the province of Pinar del Rio, Cuba. A number of specimens show more or less abundant MVs cross-cutting the groundmass, but no verifiable occurrence of any HP mineral in Viñales has so far been reported in the literature, leading to propose a shock stage S3 (Gattacceca et al., 2020) or partly S4 (Yin and Dai, 2021).

Our study includes new textural, compositional, micro-Raman spectroscopy, and electron back-scatter diffraction (EBSD) data for the Viñales meteorite. We have so far identified – through careful study of fifteen shock-melt areas – one region in a single MV that hosts the HP phases majorite and albitic jadeite. From the HP minerals present and their textural association with melt veins, we infer constraints on the pressure-temperature conditions experienced by Viñales during impact. Our findings contribute to the record of physical conditions of impacts recorded by the L-chondrites in general.

* Corresponding author.
E-mail address: ibaziotis@aua.gr (I.P. Baziotis).

https://doi.org/10.1016/j.icarus.2022.115326
Received 13 August 2022; Received in revised form 19 October 2022; Accepted 20 October 2022
Available online 25 October 2022

2. Material and analytical methods

2.1. Material

One polished mount (VIN19), prepared from a sample of the Viñales meteorite obtained from a private collection, was investigated for shock indicators with special attention to the MVs. Fifteen distinct areas located in nine MVs were analyzed for their texture and mineral chemistry (Fig. 1). Several regions were studied with spatially correlated micro-Raman spectroscopy and electron microscopy; one site, so far, has been identified as a host for two HP phases in this meteorite (Fig. 1B). Additionally, two polished thin sections (NHMW-O1166 and NHMW-O1192) from the Natural History Museum Vienna were investigated by optical microscopy for the key petrographic features used in shock stage classification schemes (see Fritz et al., 2017; Stöffler et al., 1991, 2018). Furthermore, we inspected the remnant of the meteorite chip from which one thin section (NHMW-O1166) was cut (Fig. 1A).

2.2. Analytical methods

We used transmitted and reflected light microscopy to characterize color, texture, and likely mineralogy of the different phases large enough to be resolved optically. Furthermore, optical microscopy was used to evaluate the bulk-rock deformation features associated with the shock stage experienced by the meteorite. Whole high-resolution thin sections scans were obtained using a uScopeGX-10 digital microscope scanner from Microscopes International at the Natural History Museum Vienna (Austria). Field-emission scanning electron microscopy used a JEOL JSM-IT300LV at the University of Münster, Germany, and a Zeiss 1550VP at California Institute of Technology (Caltech), USA, equipped with EBSD for determination of crystal structure. Mineral chemistry was determined with electron probe microanalyzers (EPMA), a JEOL JXA 8900 at Agricultural University of Athens, Greece, and a JEOL JXA 8530F at University of Münster. We also used a Renishaw InVia Confocal Raman microscope at the Mineral Spectroscopy Laboratory at Caltech. The 514 nm laser was set to <2 mW power to avoid laser damage. Each spectrum in the map was collected for 5 s with a 3000 line/mm diffraction grating, spanning Raman shifts of 200–1100 cm^{-1}.

3. Results

The meteorite chip is 3–5 mm thick and we were able to trace many of the complex melt veins around the edge and the back side of the rock. This suggests that the melt veins are tabular in shape and that they intersect the plane of section at a high angle, such that the observed width of the melt veins on the plane of the section is close to the true thickness of the veins.

3.1. Petrography of groundmass

The Viñales meteorite shows a light-colored interior, typical of an L6 ordinary chondrite, surrounded by a thin, dark fusion crust and cut by a network of dark veins (Fig. 1A). Most chondrules are poorly defined and a few delineated ones show a wide variety of textures, including porphyritic olivine-pyroxene, porphyritic olivine, and barred olivine. The average chondrule size is in the range of ~0.9–1.1 mm (Figs. 1, S1, S2). Abundant irregular or planar fractures are found in olivine and pyroxene, with less common fracturing of plagioclase (Figs. 2, 3).

3.1.1. Olivine

Olivine ($Fo_{75.1–75.6}$) is the predominant mineral in the groundmass of Viñales. It exhibits various deformation-related features such as irregular fractures, planar fractures, undulatory extinction, and mosaicism (Figs. 2, 3). Planar microstructures, interpreted as planar deformation features are present, but rare, in both polished thin sections (Figs. 2E, 3B). The density of these shock-related features in olivine varies considerably in the two thin sections studied. Olivine has variable crystal sizes in the range of 100–600 μm.

3.1.2. Pyroxene

Pyroxene ($En_{77.7–78.0}Fs_{20.2–21.2}Wo_{1.1–1.8}$) shows both planar and irregular fractures and moderate degrees of mosaicism (Figs. 2, 3).

3.1.3. Plagioclase

In transmitted light, the plagioclase in Viñales is always anisotropic; we have not identified diaplectic glass in either thin section. Undulatory extinction of plagioclase is common in the MV-bearing thin section NHMW-O1166 (Fig. 2H) but rare in section NHMW-O1192 (Fig. 3F). The plagioclase in Viñales has a composition of $Ab_{88.2–89.7}An_{8.0–9.8}Or_{1.8–2.3}$.

3.2. Melt veins

Numerous dark MVs cross-cut the light-colored lithology of our samples, commonly associated with L6 type. The investigated polished mount (VIN19) shows at least nine subparallel MVs, ranging from 50 up to 600 μm in thickness on the section surface, as well as a few thinner (≤40 μm thick) veins at an angle to the main ones. At this stage it is unclear whether they are the product of a single or multiple impacts. The MVs contain equigranular to anhedral silicate mineral grains, host-rock clasts, plus small (1–3 μm wide) rounded blebs of Fe—Ni metal and troilite as the main components. In a few cases, elongated oxides (chromite) occur near the edges of the MVs.

Although no HP minerals have previously been reported in the Viñales meteorite, we observed and characterized two HP minerals in VIN19: majoritic garnet and albitic jadeite (Fig. 4). A Raman spectrum, obtained from a grain (~2–3 μm in diameter) located within MV1-3b displays the characteristic major peak at ~925 cm^{-1} and minor peak at ~583 cm^{-1} reported from both synthetic and natural majorite (Fig. 5A). The EBSD pattern collected from the same point can be indexed only with the garnet structure (Fig. 5B). The EPMA compositions of five grains in this area, with these Raman and EBSD characteristics, show nearly end-member majorite composition, $Ca_{0.15}Mg_{2.96}Fe_{0.55}Al_{0.41}Si_{3.87}O_{12}$.

Within a Na-rich melt pool adjacent to the majorite-bearing melt vein, we also identified small crystals, <1–2 μm in diameter, with irregular shape, as albitic jadeite. The EPMA analysis yields the empirical formula $(Na_{0.52}Ca_{0.06}Mg_{0.04}K_{0.01}\square_{0.37})^{M2}(Al_{0.75}Si_{0.26})^{M1}Si_2O_6$, with Ca# [100 × Ca/(Ca + Na)] of 10.2. The M2 vacancy and excess Si on M1 show that this is albitic jadeite (Baziotis et al., 2022b; Ma et al., 2020, 2022). The Raman spectrum is similar to other reported instances of albitic jadeite (Baziotis et al., 2022b), with distinct peaks at ~700, 375, and 381 cm^{-1} (Fig. 6). Unfortunately, the $[Si_2O_6]^{4-}$ vibration region, a doublet at ~988 and ~ 1034 cm^{-1} in stoichiometric jadeite that merges into a single broad peak in albitic jadeite, was not observed here. No EBSD signal could be obtained from this beam-sensitive material.

4. Discussion

4.1. Shock conditions and garnet barometry

The presence of HP mineral phases in MVs constrains the shock conditions of the Viñales meteorite. If a part of the melt veins reached peak temperatures above the liquidus of the matrix material and maintained that state long enough to reach complete melting, then the MV would have evolved according to the liquidus relations of a cooling chondritic liquid. The texture of the MV hosting the majoritic garnet suggests crystallization from a liquid, indicated by the equigranular crystal shape and 120° triple junctions (Fig. 4F). As such, the measured composition of majorite indicates likely crystallization conditions of 17–20 GPa and 1800–2100 °C (Tomioka et al., 2016). True jadeite, present in some meteorites (Miyahara et al., 2013; Ohtani et al., 2017),

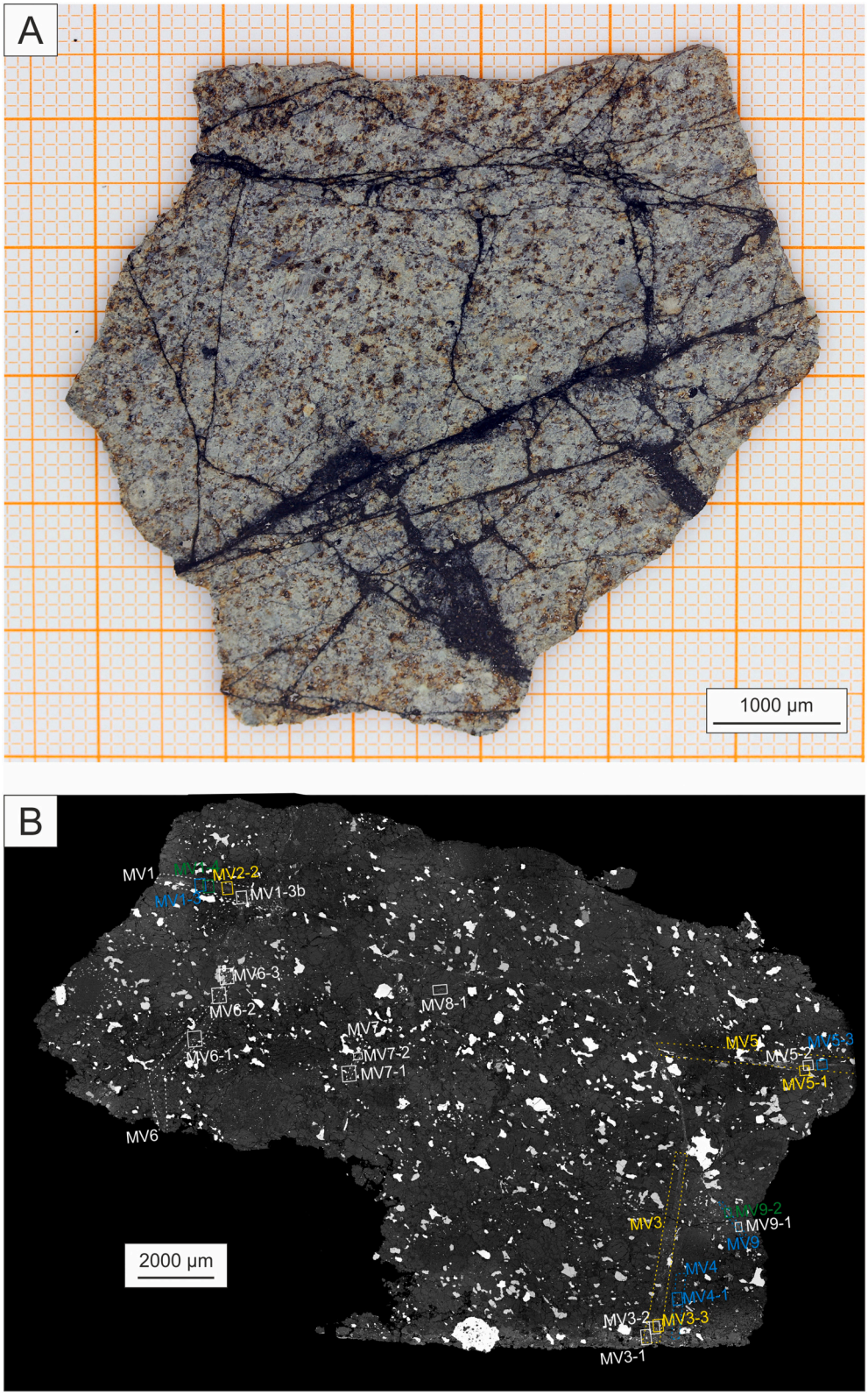

Fig. 1. (A) Macrophotograph of a large thin slice of Viñales (NHMW-O2400) showing a complex network of shock melt veins. (B) Back-scattered electron mosaic of Viñales from the polished mount (VIN19) showing the nine shock MVs examined by Raman spectroscopy. Site MV1-3b (upper left corner) contains the two HP phases reported in this study.

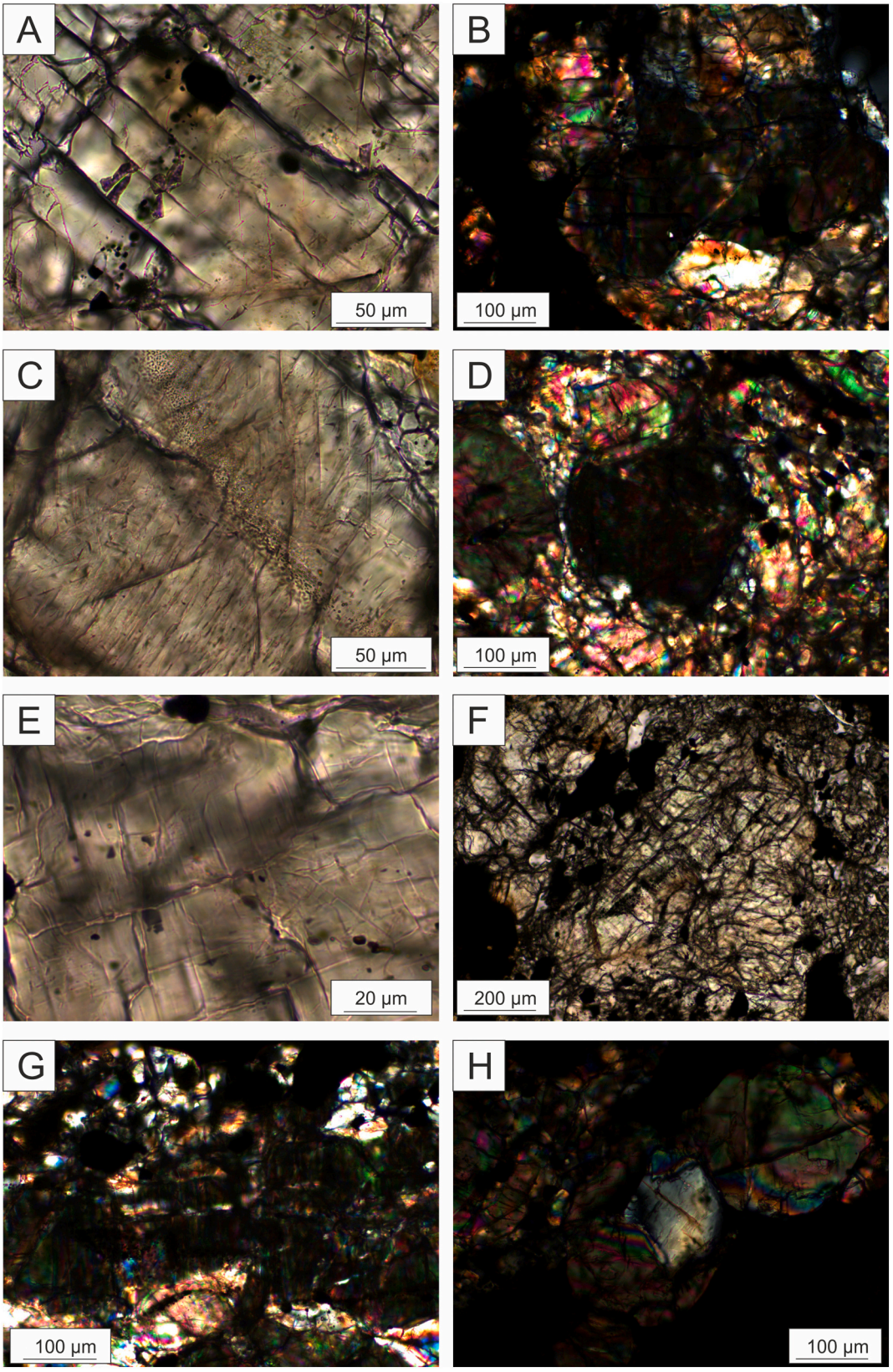

Fig. 2. Optical features of Viñales thin section NHMW-O1166: (A) one set of planar fractures in olivine (PPL); (B) moderate to strong mosaicism in olivine (XPL); (C) three sets of planar fractures in olivine (PPL); (D) weak mosaicism in olivine (XPL); (E) planar fractures (2 sets) and planar microstructures (also 2 sets; possible planar deformation features) in olivine (PPL); (F) pyroxene with irregular and planar fractures (PPL); (G) pyroxene at extinction to show mosaicism (XPL); (H) plagioclase undulatory extinction (XPL). See Fig. S1 for image positions. PPL = plane-polarized transmitted light. XPL = cross-polarized transmitted light.

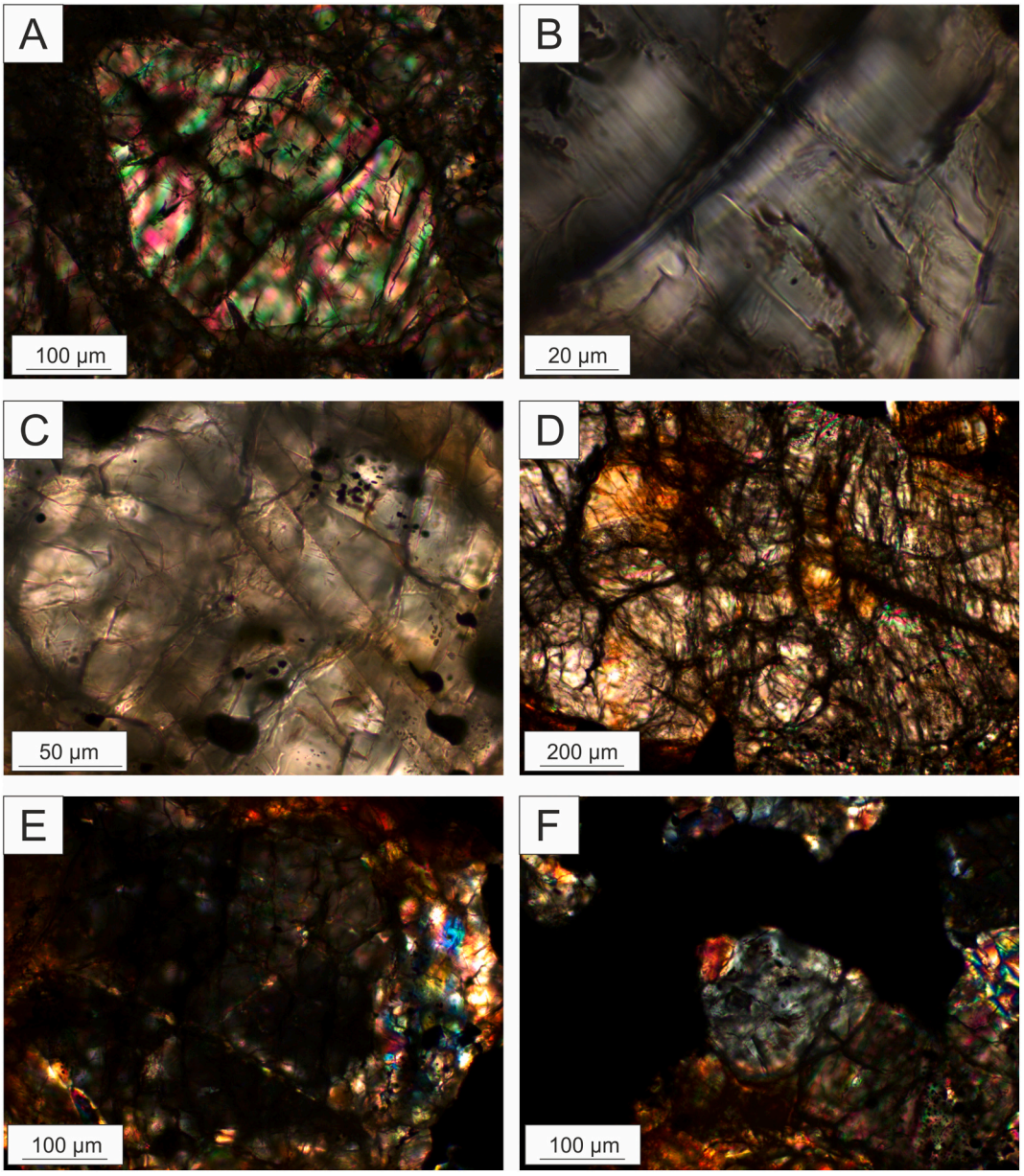

Fig. 3. Optical features of Viñales thin section NHMW-O1192: (A) olivine crystal with irregular fractures and one set of planar microstructures (possible planar deformation features; not visible on this overview microphotograph, but enlarged in B) (XPL); (B) enlarged view of the planar microstructures (PPL); (C) one set of planar fractures in an olivine crystal that exhibits undulatory extinction (PPL); (D) large pyroxene with irregular and planar fractures and undulatory extinction (XPL); (E) pyroxene with mosaicism, rare in this section; (F) typical birefringent plagioclase with undulatory extinction. See Fig. S2 for image positions.

can yield a pressure-temperature constraint given the known stability field of $NaAlSi_2O_6$ jadeite. The Raman spectra and composition from the Na-rich fine-grained region in MV3-1b of Viñales indicate a jadeite-like pyroxene, but the non-stoichiometric composition currently precludes the use of the jadeite stability field as a pressure-temperature constraint (Baziotis et al., 2022b). To date there are no experimental data on synthesis or recovery of albitic jadeite. Inferences from assemblages of HP minerals that have been found to coexist with albitic jadeite suggest that it probably forms at 18–22 GPa (Ma et al., 2022), as implied here by the coexistence with near end-member majorite. This range is consistent with the absence of lingunite in Viñales, which suggests maximum pressure < 21 GPa, the threshold for formation of lingunite (Gasparik, 1989; Liu and El Goresy, 2007).

The sensitivity of majorite composition to pressure has been calibrated by Collerson et al. (2010) and Wijbrans et al. (2016). In particular, Collerson et al. (2010) expressed the pressure estimate for majoritic garnet by:

$$P\ (GPa) = 5.78 + 18.23 \times X^{Cat}Mj, \quad (1)$$

where $X^{Cat}Mj$ represents the average value of two estimates of the majorite cation fraction, $X^{Cat}Mj_{(1)} = {}^{IV,VI}(Si + Ti) - 3 + {}^{VIII}Na$ and $X^{Cat}Mj_{(2)} = [1–0.5 \times {}^{VI}(Al + Cr)] + {}^{VIII}M_A^{2+}$. The EPMA analysis of Viñales majorite, converted to cation mole fractions on the crystallographic sites, give pressure of 21.0 ± 0.3 GPa. Although Wijbrans et al. (2016) proposed two empirical barometers for majoritic garnet in peridotitic and eclogitic compositions, the peridotite calibration does not extend above 3.3 Si atoms per formula unit and the eclogitic calibration is based on majorite with very different chemistry from that in Viñales. The pressure estimate from the Collerson et al. (2010) calibration is in good agreement with the peak shock pressure inferred from static experiments on the liquidus field of majorite in chondritic melt

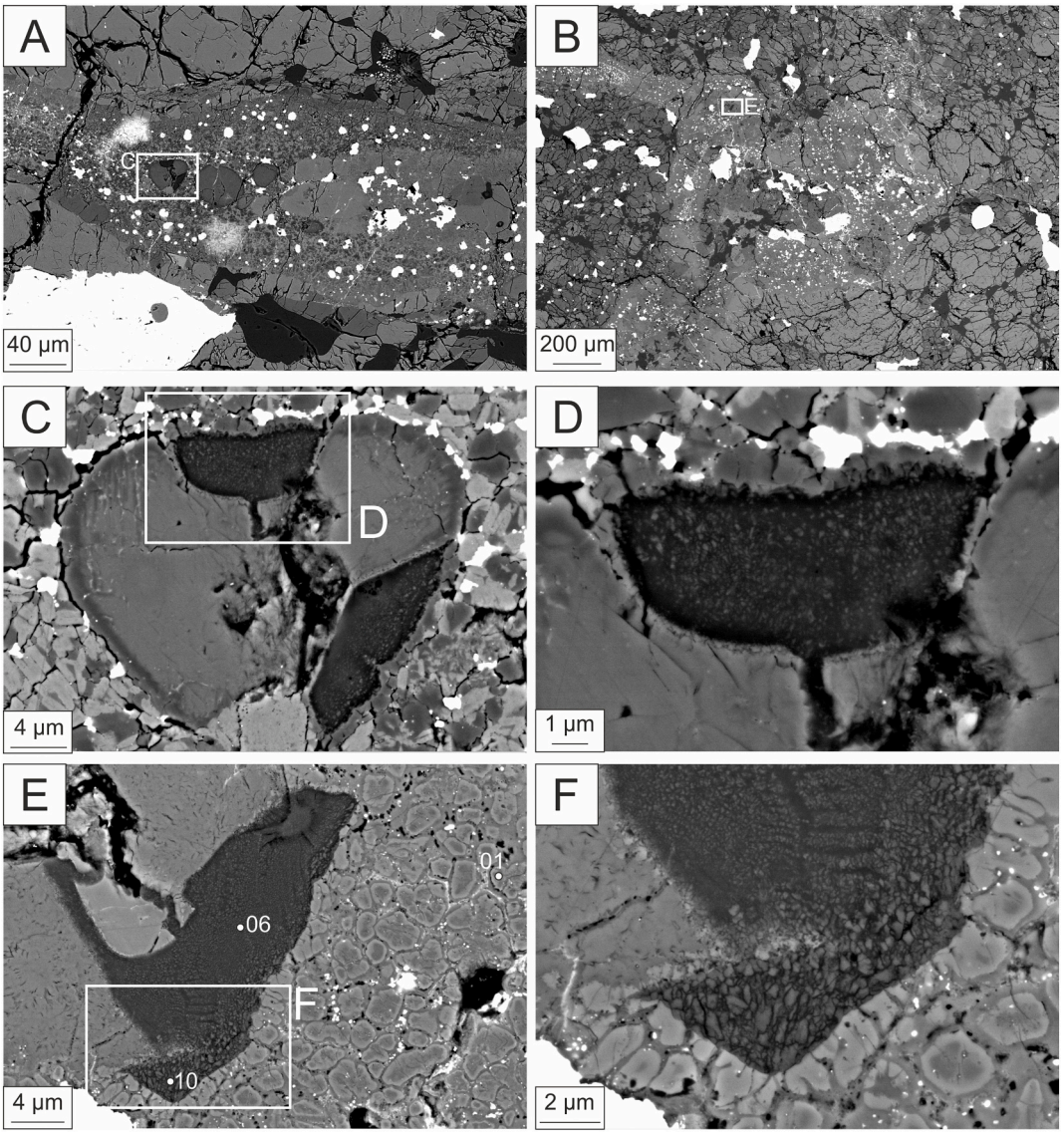

Fig. 4. (A) Site MV1-3a, hosting only low-pressure phases, enlarged in (C) and (D). (B) Site MV3-1b, hosting the HP phases, enlarged in (E) and (F). (C) A heart-shaped composite clast in site MV1-3a. (D) Enlarged area of (C) showing likely albitic jadeite. (E) The locations of Raman acquisitions indicating HP phases majorite (#01) and albitic jadeite (#06, #10). (F) Enlarged area of (E), showing a clast consisting of irregular, fine-grained crystals of albitic jadeite. The nearby matrix of the MV consists of equigranular dark majorite with brighter Fe-rich rim.

compositions.

4.2. Thermal history and preservation of HP phases

Recovery of high-pressure phases in shock melt veins generally requires that a local high temperature region, driven above its liquidus presumably by shock collapse of porosity or by shear localization, cools by loss of heat to adjacent regions while still at elevated pressure. In the early stages after the passage of a shock front, the melt flows turbulently and heat transport is dominated by advection. However, this turbulence dissipates quickly and most of the subsequent cooling path can be approximated (or at least bounded) by a conductive model that gives an upper bound to cooling time. Two-dimensional Finite Element Heat Transfer (FEHT) modeling (Klein et al., 2003) was applied to estimate the maximum lifetime of selected shock melt veins in Viñales, focusing on the vein where majorite and albitic jadeite were found. Key parameters of the model include the thickness of the vein and the thermal diffusivity of the meteorite matrix. We obtained densely sampled measurements of vein thickness in order to develop a robust estimate of the typical width; several veins yielded clusters of width measurements near 20 μm, whereas MV3 also has several segments close to 200 μm wide. Hence, we modeled the evolution of both 20 and 200 μm thick melt veins. The initial density of Viñales, based on relative mineral modes, is estimated at 3.240 g cm^{-3} and a typical ordinary chondrite Hugoniot then indicates that the density at 16 GPa is about 3.653 g cm^{-3} (Walsh and Christian, 1955; Stöffler et al., 1988; Ahrens and Johnson, 1995a, 1995b). We considered values of thermal conductivity of 3, 5, and 10 W $\times$ m^{-1} $\times$ K^{-1}; the lowest value yields the longest quench time (Xie et al., 2006). The specific heat capacities of both matrix and melt were set at 846 J $\times$ kg^{-1} $\times$ K^{-1} (Turcotte and Schubert, 2014). The initial temperature of the matrix was set at 27 °C, whereas the shock melt was set at 2300 °C. The temperature relaxation was then calculated as a function of time and distance in a two-sided slab geometry.

In a 20 μm wide vein, the outermost 3 μm begins crystallizing (<2000 °C) almost instantaneously after the melting, the outer 6 μm on both sides begins crystallizing within 30 μs, and the center of the vein crystallizes within 40 μs. Thus, veins of such a thickness were probably fully crystallized while still under high pressure. In a 200 μm wide vein,

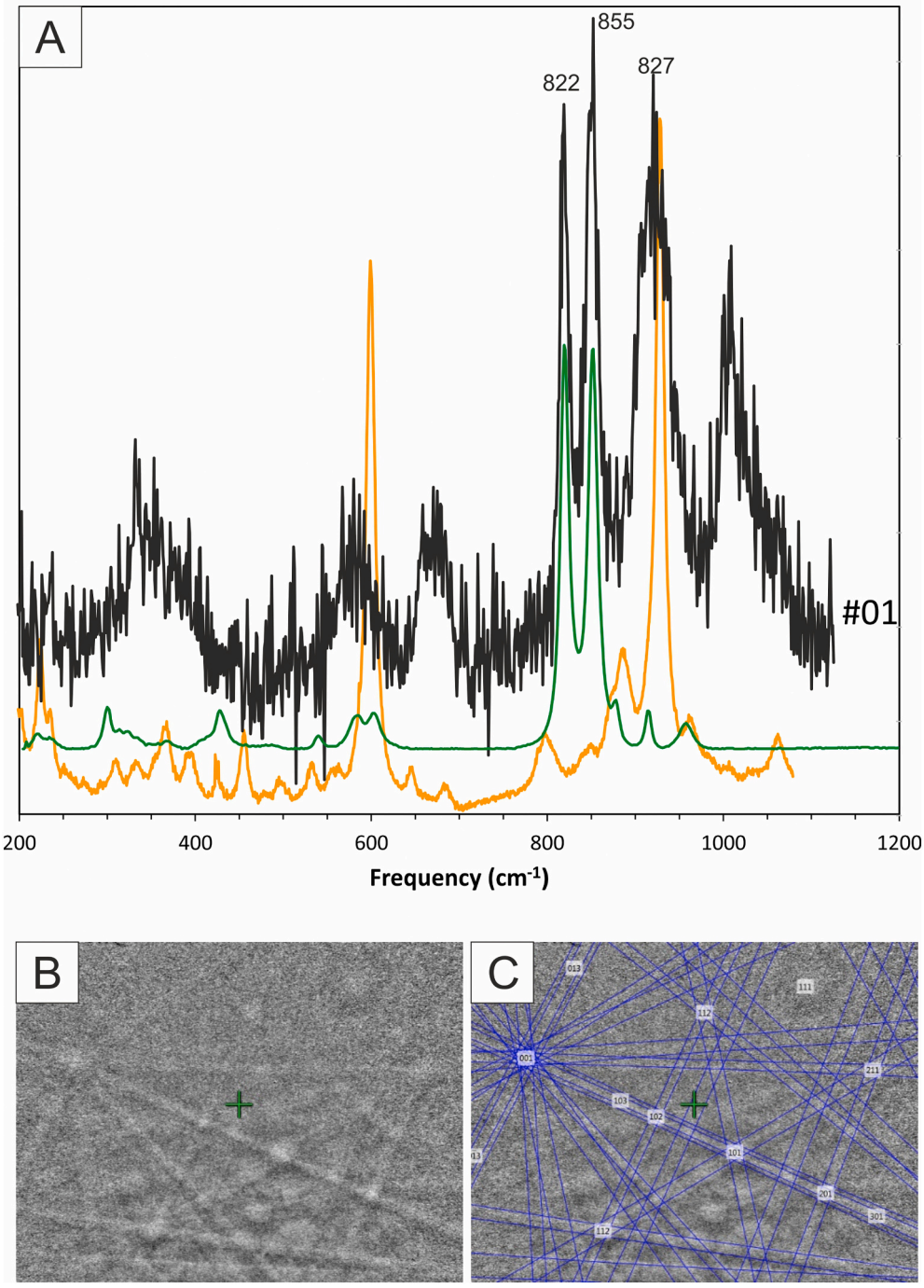

Fig. 5. (A) Selected Raman spectrum of the majorite in Viñales from site MV1-3b, compared to reference spectrum for olivine (green line; RRUFF X050088), and majorite (orange line; Handbook of Raman Spectra; Rauch et al., 1996). (B) EBSD pattern spatially correlated with Raman spectrum MV1-3b-01 given in A. (C) Indexing of the EBSD pattern as majorite. (For interpretation of the references to color in this figure legend, the reader is referred to the web version of this article.)

models show that the outermost 30 μm zones on both sides of the vein would start to crystallize within 500 μs, the outermost 60 μm zones on both sides begin crystallizing in 1 ms, and the center of the vein would start crystallizing within 2 ms after melting. Translating these times into impactor sizes introduces additional uncertainty, but impacts between chondritic bodies that achieve pressures of 16 GPa at the center of impact site involve encounter velocities of at least ~1.5 km s^{-1}. A two-way travel-time criterion for shock release implies minimum object sizes of 1 to 6 m to achieve preservation of albitic jadeite and majoritic garnet in 20 to 200 μm wide shock melt veins. As such, our results are consistent with the recent study of Ciocco et al. (2022) that L chondrites may have either (1) separated from the parent body before its catastrophic disruption and been shocked by secondary impacts among smaller objects or (2) originated from various depths in the parent body that experienced a range of shock time scales.

4.3. Shock stage classification

Several systems of criteria have been used in the last few decades to define shock stages and for ordinary chondrites the pressures marking the boundaries between stages (Stöffler et al., 1991; Chen et al., 1996; Sharp and DeCarli, 2006; Stöffler and Grieve, 2007; Fritz et al., 2017;

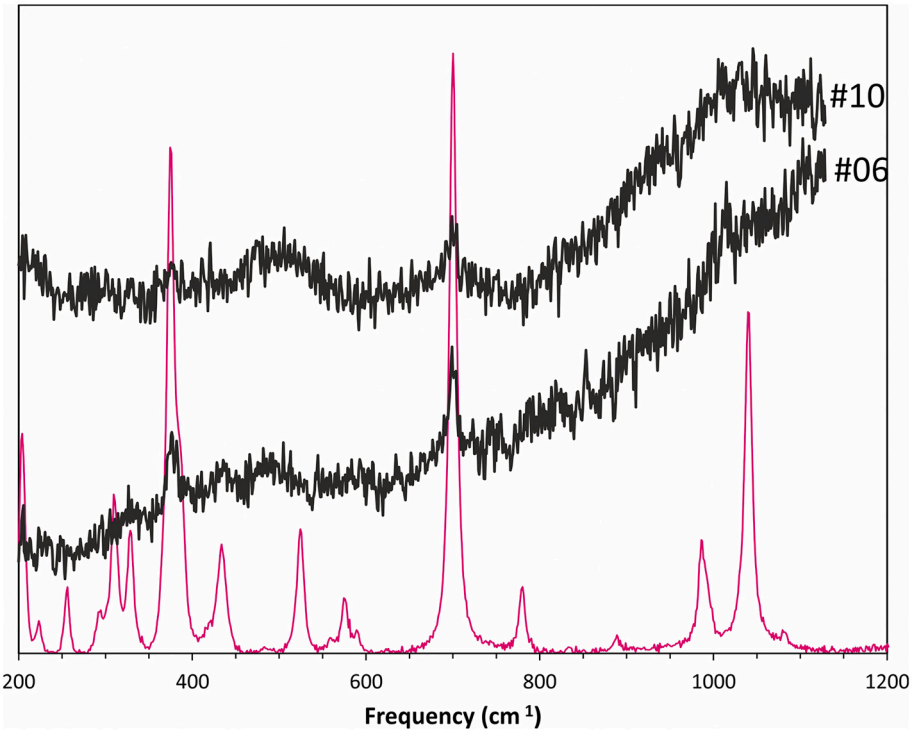

Fig. 6. Selected Raman spectra of the albitic jadeite in Viñales from site MV1-3b, compared to reference spectrum for jadeite (RRUFF R050220.2).

Stöffler et al., 2018). Important clarifications of the shock pressures associated with the classification of ordinary chondrites have been published recently by Bischoff et al. (2019) and Hu and Sharp (2022), but the shock stages of L6 meteorites remain controversial.

4.3.1. Shock classification of the Viñales meteorite

Observations of HP mineral phases, i.e., majorite and albitic jadeite, MVs, as well as shock-induced features in the matrix of Viñales are all relevant to the shock state of this meteorite. Previous works suggested shock stage S3 based on the observations of Gattacceca et al. (2020) or partly S4 based on the observations (<30% of feldspar has been transformed into maskelynite, and > 50% of olivine shows irregular fractures) of Yin and Dai (2021). In Table 1 we summarize our optical examination of two thin sections of Viñales and apply the classification schemes of both Fritz et al. (2017) and Stöffler et al. (2018). Importantly, we observe some heterogeneity among samples. One thin section (Figs. 2, S1), containing a complex network of melt veins, meets the criteria for S4 in both classification schemes. Another thin section (Figs. 3, S2), free of melt veins, is S4 according to Stöffler et al. (2018) but S3 according to Fritz et al. (2017).

4.3.2. Outstanding issues with shock stage classification

We highlight that shock stage classification of L6 chondrites remains challenging for several reasons: heterogeneity among different samples of a given meteorite, difficulty of unambiguous optical determination, different pressure estimates for the different shock stages, and poor

Table 1
Observations on Viñales meteorite from two thin sections and assignment of shock stage based on Fritz et al. (2017) and Stöffler et al. (2018).

	SOX	UE	UE & PFs	WM & PFs	SM & PDFs	Phases in melt zones	Shock stage[a]	Shock stage[b]
Thin section NHMW-O1166								
Olivine	–		+	+	+			
Pyroxene	–		+	+	–			
Plagioclase	–	+	+	–	–		**S4**	**S4**
Melt vein						–		
Melt pocket						–		
Thin section NHMW-O1192								
Olivine	–		+	+	+			
Pyroxene	–	+	+	–	–			
Plagioclase	–	+		–	–		**S3**	**S4**
Melt vein						–		
Melt pocket						–		
Polished Mount VIN19								
Melt vein						LP, Maj, Ab-Jd, Gl	**S4**	**S4**
Melt pocket						LP, Gl		

SOX: sharp optical extinction; UE: undulatory extinction; PFs: planar fractures; WM: weak mosaicism; SM: strong mosaicism; PDFs: planar deformation features; Maj: majorite; Ab-Jd: albitic jadeite; LP: low-pressure phases; Gl: glass; a: Fritz et al. (2017); b: Stöffler et al. (2018).
-: the feature is absent; +: the feature or features are present; +: the feature or features are common.

integration of HP mineral constraints together with optical criteria.

As emphasized by Bischoff et al. (2019), there is a disconnection between the accepted practice of assigning a given meteorite a single shock stage classification and the heterogeneity among different samples of some meteorites. Viñales is a good example, with one thin section containing abundant MVs and rare planar microstructures interpreted to be planar deformation features (PDFs) and another one in which no MVs are visible. Meteorite classification is often based on examination of only one thin section, but it is apparent that this can provide an incomplete picture (Bischoff et al., 2019).

Another issue is that shock classification is commonly based exclusively on optical microscopy. From a practical standpoint, optical microscopy may be the only tool available, but it requires considerable expertise to apply it correctly and in a reproducible way. Some features, e.g. PDFs, can be easily missed or misidentified. Regions of shocked meteorites that have experienced intense shock darkening may not transmit enough light to be able to identify shock features under the optical microscope. To reach robust standards for the recognition of shock stages, the classification schemes may need to be expanded to include evidence from additional analytical methods. For example, X-ray diffraction can clarify the evolution of crystal structure (Rupert et al., 2020; Imae and Kimura, 2021) with progressive shock stages. Raman spectroscopy and electron microscopy are essential for the recognition of HP minerals, whose presence or absence probably ought to be better integrated with deformation-related criteria for shock stage classification. A reliable method of shock stage assignment and understanding of the significance of HP minerals in shock classification likely calls for the paired application of qualitative optical criteria (as in Fritz et al., 2017 and Stöffler et al., 2018) and quantitative criteria as described in, e.g., Rupert et al. (2020) and Imae and Kimura (2021).

Finally, even when classification schemes agree on optical criteria — e.g., Fritz et al. (2017) and Stöffler et al. (2018) concur that S3 is marked by local development of MVs — they differ in the peak pressures that are thought to correspond to some shock features and stages. Fritz et al. (2017) concur with Stöffler et al. (1991, 2018) that the lower boundary of S3 is 5–10 GPa and the upper boundary of S3 is 15–20 GPa (with maximum post-shock temperature of 373–423 K) (Schmitt, 2000). However, Fritz et al. (2017) revise the upper boundary of S4 downwards to 25–35 GPa from the 30–35 GPa range given by Stöffler et al. (1991, 2018). The classification of Stöffler et al. (2018) also includes estimates for pre-heated targets, allowing for the transition to S5 to begin as low 20 GPa from initial temperature of 920 K. These differences are important because shock stage S4 ought to be consistent with both the formation and the preservation of HP minerals such as ringwoodite and majorite in MVs. These phases require peak pressures in the range of 17–23 GPa (Hu and Sharp, 2022), but in some cases they coexist with "maskelynite" (here we note an ambiguity in terminology, with some authors using the word maskelynite to describe both diaplectic glass formed by solid-state transformation and glass quenched from a melt; see Ferrière and Brandstätter, 2015), which is indicates pressure above 28–35 GPa in An-rich feldspar, according to some studies (e.g., Stöffler et al., 1986). For Viñales, plagioclase is mostly crystalline (generally associated with S3 or less) but the threshold shock pressure for amorphization increases towards the albite end-member. The high Ab content of plagioclase in Viñales allows for crystalline feldspar to persist into the S4 pressure range. Moreover, the cooling paths must reach low post-shock temperatures to avoid back-transformation (Hu and Sharp, 2022), which is possible from S4 but not from higher stages (Fritz et al., 2017). Equilibrium reversion of majorite to lower-pressure phases occurs along a curve that passes through 17 GPa at 1800 K and 15.5 GPa at 2500 K (Jacobs et al., 2017). However, the inference that a sample preserving majorite must have cooled rapidly enough to remain below this boundary presently lacks confidence. Kinetic decompression experiments are not available to precisely define the effective metastability limit for majorite (Hu and Sharp, 2022) and critical temperatures for garnet minerals are roughly 1300–1500 K (Thieblot et al., 1998). There are no available synthesis or reversion experiments for albitic jadeite.

4.4. Fragmentation upon atmospheric entry and shock-related features

Viñales, upon atmospheric entry, exploded and broke apart into numerous pieces. The Meteoritical Bulletin Database reports that "*Hundreds of individual samples were collected by the local residents. […] The masses of stones are in a range 2 to 1100 g. In total, about 50-100 kg of the meteorite were collected*". The fragmentation of the Viñales fall is not unusual among chondrites; for example, in one of the most spectacular events of the last few decades, the LL5 fall Chelyabinsk broke up in a similar fashion (Walton et al., 2021). The magnitude of aerodynamic stresses that drive fragmentation is most strongly dependent on meteoroid size, but the response of the meteoroid to those stresses depends on its material strength and internal structure. We speculate that fragmentation may be localized along shock melt veins and be more efficient (for a given meteoroid size) in objects containing penetrative networks of MVs upon their arrival at Earth. Popova et al. (2013) argued that shock melt vein with a segregated layer of metal may cause structural weakness by differential thermal expansion, although shock melting generally increase the material strength. Similarly, in Viñales, a high density of interconnected MVs of variable thickness is present in our studied sections (as also visible at the macroscopic scale on Fig. 1A) and in fragments studied by other researchers (e.g., Yin and Dai, 2021). Most of the MVs in Viñales feature a segregated metal-rich layer as well (Fig. 4). The weakness of strongly shocked chondritic meteorites, promoting highly fragmentary falls, may therefore be related to the catastrophic impacts that disrupted their parent bodies. Later, secondary impacts that triggered the delivery of these meteoroids to Earth (Ciocco et al., 2022) may have further weakened them with networks of fractures (Baziotis et al. 2022a, 2022b).

5. Conclusions

Pending further analyses, it is now clear that Viñales hosts minerals that formed at elevated pressure and temperature, including majorite and albitic jadeite. Hence, the investigated sections of Viñales shows features more consistent with shock stage S4 (Fritz et al., 2017; Stöffler et al., 2018; Hu and Sharp, 2022) than with the previously documented S3 (Gattacceca et al., 2020) or partly S4 (Yin and Dai, 2021). The presence of discrete melt veins indicates heterogeneity of the temperature field, likely the result of the collapse of spatially variable porosity during shock compression or slip along localized shear bands (Baziotis et al., 2018). We cannot presently define the full range of peak conditions or *P-T* paths experienced by the meteorite or rule out the recording of multiple shock events on its parent body. Priorities for future work include determining the chronology of the different shock vein generations in Viñales to place further constraints on the parent-body break up event and other impact event(s) recorded in L6 meteorites.

Declaration of Competing Interest

None.

Data availability

Please see Appendix A for complete data files.

Acknowledgements

I.B., S.X., and A.P. received support for this research from ESF and the Greek State (call code EDBM103). I.B. research received support from the SYNTHESYS Project (http://www.synthesys.info/ which is financed by European Community Research Infrastructure Action under the FP7 "Capacities" Program, covering travel and accommodation as

well as instrument time costs at the Natural History Museum Vienna (Austria). PDA acknowledged NSF award 1725349.

Appendix A. Supplementary data

Supplementary data to this article can be found online at https://doi.org/10.1016/j.icarus.2022.115326.

References

Ahrens, T.J., Johnson, M.L., 1995a. Shock wave data for minerals. Min. Phys. Crystallogr., A Handb. Phys. Const. 2, 143–184.

Ahrens, T.J., Johnson, M.L., 1995b. Shock wave data for rocks. Min. Phys. Crystallogr., A Handb. Phys. Const. 3, 35–44.

Baziotis, I., Asimow, P.D., Hu, J., Ferrière, L., Ma, C., Cernok, A., Topa, D., 2018. High pressure minerals in the Château-Renard (L6) ordinary chondrite: implications for collisions on its parent body. Sci. Rep. 8 (1), 1–16.

Baziotis, I., Xydous, S., Papoutsa, A., Hu, J., Ma, C., Klemme, S., Berndt, J., Ferrière, L., Caracas, R., Asimow, P.D., 2022a. Jadeite and related species in shocked meteorites: limitations on inference of shock conditions. Am. Mineral. 107 (10), 1868–1877.

Baziotis, I.P., Ma, C., Guan, Y., Ferrière, L., Xydous, S., Hu, J., Kipp, M.A., Tissot, F.L.H., Asimow, P.D., 2022b. Unique evidence of fluid alteration in the Kakowa ordinary chondrite. Sci. Rep. 12, 5520.

Binns, R.A., Davis, R.J., Reed, S.J.B., 1969. Ringwoodite, natural (Mg, Fe)$_2$SiO$_4$ spinel in the Tenham meteorite. Nature 221 (5184), 943–944.

Bischoff, A., Schleiting, M., Patzek, M., 2019. Shock stage distribution of 2280 ordinary chondrites—can bulk chondrites with a shock stage of S6 exist as individual rocks? Meteorit. Planet. Sci. 54 (10), 2189–2202.

Bogard, D.D., Husain, L., Wright, R.J., 1976. ^{40}Ar-^{39}Ar dating of collisional events in chondrite parent bodies. J. Geophys. Res. 81 (32), 5664–5678.

Chao, E.C.T., Fahey, J.J., Littler, J., Milton, D.J., 1962. Stishovite, SiO$_2$, a very high pressure new mineral from meteor crater, Arizona. J. Geophys. Res. 67 (1), 419–421.

Chen, M., Sharp, T.G., Goresy, A.E., Wopenka, B., Xie, X., 1996. The majorite-pyrope+ magnesiowüstite assemblage: Constraints on the history of shock veins in chondrites. Science 271 (5255), 1570–1573.

Chen, M., Shu, J., Xie, X., Mao, H.K., 2003. Natural CaTi$_2$O$_4$-structured FeCr$_2$O$_4$ polymorph in the Suizhou meteorite and its significance in mantle mineralogy. Geochim. Cosmochim. Acta 67 (20), 3937–3942.

Ciocco, M., Roskosz, M., Doisneau, B., Beyssac, O., Mostefaoui, S., Remusat, L., Leroux, H., Gounelle, M., 2022. Impact dynamics of the L chondrites' parent asteroid. Meteorit. Planet. Sci. 57 (4), 759–775.

Collerson, K.D., Williams, Q., Kamber, B.S., Omori, S., Arai, H., Ohtani, E., 2010. Majoritic garnet: A new approach to pressure estimation of shock events in meteorites and the encapsulation of sub-lithospheric inclusions in diamond. Geochim. Cosmochim. Acta 74 (20), 5939–5957.

Ferrière, L., Brandstätter, F., 2015. What is maskelynite? Back to the original description and thin sections in which it was first described. Meteorit. Planet. Sci. 50 (s1), A126.

Fritz, J., Greshake, A., Fernandes, V.A., 2017. Revising the shock classification of meteorites. Meteorit. Planet. Sci. 52 (6), 1216–1232.

Gasparik, T., 1989. Transformation of enstatite—diopside—jadeite pyroxenes to garnet. Contrib. Mineral. Petrol. 102 (4), 389–405.

Gattacceca, J., McCubbin, F.M., Bouvier, A., Grossman, J.N., 2020. The Meteoritical bulletin, no. 108. Meteorit. Planet. Sci. 55 (5), 1146–1150.

Heymann, D., 1967. On the origin of hypersthene chondrites: ages and shock effects of black chondrites. Icarus 6 (1–3), 189–221.

Hu, J., Sharp, T.G., 2022. Formation, preservation and extinction of high-pressure minerals in meteorites: temperature effects in shock metamorphism and shock classification. Progr. Earth Planet. Sci. 9 (1), 1–22.

Imae, N., Kimura, M., 2021. Quantitative determination of the shock stage of L6 ordinary chondrites using X-ray diffraction. Am. Mineral. 106 (9), 1470–1479.

Jacobs, M.H., Schmid-Fetzer, R., van den Berg, A.P., 2017. Phase diagrams, thermodynamic properties and sound velocities derived from a multiple Einstein method using vibrational densities of states: an application to MgO–SiO$_2$. Phys. Chem. Miner. 44 (1), 43–62.

James, O., 1969. Jadeite: shock-induced formation from oligoclase, Ries crater, Germany. Science 165, 1005–1008.

Klein, S., Beckman, W.A., Myers, G.E., 2003. FEHT: A Finite Element Analysis Program for the Microsoft Windows Operating System. F-Chart Software.

Korochantseva, E.V., Trieloff, M., Lorenz, C.A., Buykin, A.I., Ivanova, M.A., Schwarz, W. H., Jessberger, E.K., 2007. L-chondrite asteroid breakup tied to Ordovician meteorite shower by multiple isochron ^{40}Ar-^{39} Ar dating. Meteorit. Planet. Sci. 42 (1), 113–130.

Liu, L.-G., 1978. High-pressure phase transformations of albite, jadeite and nepheline. Earth Planet. Sci. Lett. 37 (3), 438–444.

Liu, L.G., El Goresy, A., 2007. High-pressure phase transitions of the feldspars, and further characterization of lingunite. Int. Geol. Rev. 49 (9), 854–860.

Ma, C., Tschauner, O., Kong, M., Beckett, J.R., Greenberg, E., Prakapenka, V.B., Lee, Y., 2020. Discovery of a Highly-defective, Shock-induced, High-Pressure Albitic Jadeite, (Na,Ca,□$_{1/4}$)(Al,Si)Si$_2$O$_6$: Natural Occurrence of a Clinopyroxene with Excess Si. 51st Lunar and Planetary Science Conference, Abstract #1712.

Ma, C., Tschauner, O., Kong, M., Beckett, J.R., Greenberg, E., Prakapenka, V.B., Lee, Y., 2022. A high-pressure, clinopyroxene-structured polymorph of albite in highly shocked terrestrial and meteoritic rocks. Am. Mineral. 107 (4), 625–630.

Mason, B., Nelen, J., White Jr., J.S., 1968. Olivine-garnet transformation in a meteorite. Science 160 (3823), 66–67.

Miyahara, M., Ozawa, S., Ohtani, E., Kimura, M., Kubo, T., Sakai, T., Hirao, N., 2013. Jadeite formation in shocked ordinary chondrites. Earth Planet. Sci. Lett. 373, 102–108.

Ohtani, E., Ozawa, S., Miyahara, M., 2017. Jadeite in shocked meteorites and its textural variations. J. Mineral. Petrol. Sci. 112 (5), 247–255.

Popova, O.P., Jenniskens, P., Emel'yanenko, V., Kartashova, A., Biryukov, E., Khaibrakhmanov, S., The Chelyabinsk Airburst Consortium, 2013. Chelyabinsk airburst, damage assessment, meteorite recovery, and characterization. Science 342 (6162), 1069–1073.

Putnis, A., Price, G.D., 1979. High-pressure (mg, Fe)$_2$SiO$_4$ phases in the Tenham chondritic meteorite. Nature 280 (5719), 217–218.

Rauch, M., Keppler, H., Hafner, W., Poe, B., Wokaun, A., 1996. A pressure-induced phase transition in MgSiO$_3$-rich garnet revealed by Raman spectroscopy. Am. Mineral. 81 (9–10), 1289–1292.

Rupert, A.N., McCausland, P.J., Flemming, R.L., 2020. Ordinary chondrite shock stage quantification using in situ 2-DX-ray diffraction of olivine. Meteorit. Planet. Sci. 55 (10), 2224–2240.

Sazonova, L.V., Fel'dman, V.I., Kozlov, E.A., Dubrovinskaya, N.A., Dubrovinskii, L.S., 2006. Genesis of ringwoodite during metamorphism induced by impact waves: experimental data. Geochem. Int. 44 (2), 137–142.

Schmitt, R.T., 2000. Shock experiments with the H6 chondrite Kernouvé: Pressure calibration of microscopic shock effects. Meteorit. Planet. Sci. 35 (3), 545–560.

Schmitz, B., Tassinari, M., Peucker-Ehrenbrink, B., 2001. A rain of ordinary chondritic meteorites in the early Ordovician. Earth Planet. Sci. Lett. 194 (1–2), 1–15.

Sharp, T.G., DeCarli, P.S., 2006. Shock effects in meteorites. Meteorit. Early Solar Syst. II 943, 653–677.

Sharp, T.G., Lingemann, C.M., Dupas, C., Stoffler, D., 1997. Natural occurrence of MgSiO$_3$-ilmenite and evidence for MgSiO$_3$-perovskite in a shocked L chondrite. Science 277 (5324), 352–355.

Stöffler, D., Grieve, R.A.F., 2007. Impactites. In: Fettes, D., Desmons, J. (Eds.), Metamorphic Rocks: A Classification and Glossary of Terms, Recommendations of the International Union of Geological Sciences. Cambridge University Press, Cambridge, UK (pp. 82–92, 111–125, and 126–242).

Stöffler, D., Ostertag, R., Jammes, C., Pfannschmidt, G., Sen Gupta, P.R., Simon, S.B., Papike, J.J., Beauchamp, R.H., 1986. Shock metamorphism and petrography of the Shergotty achondrite. Geochim. Cosmochim. Acta 50 (6), 889–903.

Stöffler, D., Bischoff, A., Buchwald, V., Rubin, A.E., 1988. Shock effects in meteorites. In: Kerridge, J.F., Matthews, M.S. (Eds.), Meteorites and the Early Solar System. University of Arizona Press, Tucson, pp. 165–202.

Stöffler, D., Keil, K., Scott, E.R.D., 1991. Shock metamorphism of ordinary chondrites. Geochim. Cosmochim. Acta 55 (12), 3845–3867.

Stöffler, D., Hamann, C., Metzler, K., 2018. Shock metamorphism of planetary silicate rocks and sediments: proposal for an updated classification system. Meteorit. Planet. Sci. 53 (1), 5–49.

Thieblot, L., Roux, J., Richet, P., 1998. High-temperature thermal expansion and decomposition of garnets. Eur. J. Mineral. 7–16.

Tomioka, N., Miyahara, M., Ito, M., 2016. Discovery of natural MgSiO$_3$ tetragonal garnet in a shocked chondritic meteorite. Sci. Adv. 2 (3), e1501725.

Tschauner, O., Ma, C., Beckett, J.R., Prescher, C., Prakapenka, V.B., Rossman, G.R., 2014. Discovery of bridgmanite, the most abundant mineral in earth, in a shocked meteorite. Science 346 (6213), 1100–1102.

Turcotte, D.L., Schubert, G., 2014. Geodynamics, 3rd edition. Cambridge University Press, p. 656.

Walsh, J.M., Christian, R.H., 1955. Equation of state of metals from shock wave measurements. Phys. Rev. 97, 1544–1556.

Walton, C.R., Baziotis, I., Černok, A., Ferrière, L., Asimow, P.D., Shorttle, O., Anand, M., 2021. Microtextures in the Chelyabinsk impact breccia reveal the history of phosphorus-olivine-assemblages in chondrites. Meteorit. Planet. Sci. 56 (4), 742–766.

Wijbrans, C.H., Rohrbach, A., Klemme, S., 2016. An experimental investigation of the stability of majoritic garnet in the Earth's mantle and an improved majorite geobarometer. Contrib. Mineral. Petrol. 171 (5), 1–20.

Xie, X., Minitti, M.E., Chen, M., Mao, H.K., Wang, D., Shu, J., Fei, Y., 2002. Natural high-pressure polymorph of merrillite in the shock veins of the Suizhou meteorite. Geochim. Cosmochim. Acta 66 (13), 2439–2444.

Xie, Z., Sharp, T.G., DeCarli, P.S., 2006. High-pressure phases in a shock-induced melt vein of the Tenham L6 chondrite: constraints on shock pressure and duration. Geochim. Cosmochim. Acta 70, 504–515.

Yin, F., Dai, D., 2021. Petrology and mineralogy of the Viñales meteorite, the latest fall in Cuba. Sci. Prog. 104 (2) (00368504211019859).

Yin, Q.Z., Zhou, Q., Li, Q.L., Li, X.H., Liu, Y., Tang, G.Q., Jenniskens, P., 2014. Records of the Moon-forming impact and the 470 Ma disruption of the L chondrite parent body in the asteroid belt from U-Pb apatite ages of Novato (L6). Meteorit. Planet. Sci. 49 (8), 1426–1439.